https://doi.org/10.5194/egusphere-2025-2630
Preprint. Discussion started: 8 August 2025

HONO Formation Mechanisms and Impacts on Ambient Oxidants in Coastal Regions of Fujian, China

Haoran Zhang[1], Chengchun Shi[2,3], Chuanyou Ying[1,4], Shengheng Weng[5], Erling Ni[2,3], Lanbu Zhao[1], Peiheng Yang[1], Keqin Tang[6], Xueyu Zhou[1], Chuanhua Ren[1], Tengyu Liu[1], Mengmeng Li[1], Nan Li[6], Xin Huang[1*]

[1] School of Atmospheric Sciences, Nanjing University, Nanjing, 210023, China
[2] Fujian Academy of Environmental Sciences, Fuzhou, 350013, China
[3] Fujian Key Laboratory of Environmental Engineering, Fuzhou, 350013, China
[4] Fuzhou Research Academy of Environmental Sciences, Fuzhou, 350013, China
[5] Fujian Institute of Meteorological Sciences, China Meteorological Administration, Fuzhou, 350001, China
[6] Jiangsu Key Laboratory of Atmospheric Environment Monitoring and Pollution Control, Jiangsu Collaborative Innovation Center of Atmospheric Environment and Equipment Technology, School of Environmental Science and Engineering, Nanjing University of Information Science & Technology, Nanjing, 210044, China

Correspondence to: Xin Huang (xinhuang@nju.edu.cn)

Abstract. Nitrous acid (HONO) is a vital precursor of hydroxyl radicals (OH) in the troposphere, leading to the formation of secondary air pollutants, including ozone (O_3) and secondary aerosols. Previous studies have mainly focused on investigating the chemical fate of HONO in polluted urban areas of China and found a general diurnal variation featuring the minimum concentration around noon. However, this study reported a significantly higher daytime HONO concentrations based on one-month measurement during May of 2024 over the coastal regions of Fujian in southeastern China. Using an updated chemical transport model, we captured the magnitude and temporal variation observed in coastal HONO levels, and improved the model performance on diurnal patterns of the NO_2 and O_3. Further process analysis revealed that two light-dependent chemical sources, i.e., the heterogeneous uptake of NO_2 on the ground surface and NO_x photo-oxidation, were the main contributors to HONO formation, particularly at high concentrations around noon in the presence of persistent intensive solar radiation. In addition, we assessed that shipping emissions contributed 20% to the midday HONO production rate in coastal regions. Subsequently, model results indicated that HONO photolysis accounted for 34% of primary OH sources during the daytime. Model sensitivity experiments demonstrated that incorporating multiple HONO sources increased the daily maximum OH and average O_3 concentrations by 61% and 44%, respectively, in coastal regions. Overall, this study highlights the unique formation mechanisms of HONO and its significant contribution to ambient oxidants in typical coastal regions.

Keywords. Nitrous acid, Ozone, OH radicals, Southeast China, WRF-Chem

https://doi.org/10.5194/egusphere-2025-2630
Preprint. Discussion started: 8 August 2025

1 Introduction

Nitrous acid (HONO) is an unstable reactive nitrogen species. It can be generated through various formation pathways, such as direct emissions from combustion-related processes, soils, and fertilization (Kurtenbach et al., 2001; Oswald et al., 2013; Su et al., 2011; Tan et al., 2023), the homogeneous reaction between NO and OH (R1) (Sarwar et al., 2008), light-enhanced NO_2 heterogeneous uptake on solid surfaces (R2) (Finlayson-Pitts et al., 2003; George et al., 2015; Kim et al., 2024), and photolysis of particulate nitrate aerosols (R3) (Ye et al., 2016, 2017). In addition, a recent laboratory study also reported that the photo- and dark-oxidation of nitrogen oxides (NO_x) could significantly contribute to HONO formation (Song et al., 2023).

$$NO + OH \rightarrow HONO \quad (R1)$$

$$2NO_2 + H_2O + h\nu \xrightarrow{Surface} HONO + HNO_3 \quad (R2)$$

$$pNO_3^- + h\nu \rightarrow 0.67\ HONO + 0.33\ NO_2 \quad (R3)$$

In the presence of sunlight, HONO can rapidly undergo photodissociation (R4) to yield NO and OH radicals (Seinfeld and Pandis, 2016). This photolytic process of HONO plays a vital role in maintaining the atmospheric oxidizing capacity (AOC) and facilitating the formation of secondary air pollutants (Kleffmann et al., 2005). For example, during the daytime, the oxidation of NO_2 by OH usually results in the production of nitric acid (HNO_3) (R5), which subsequently reacts with ammonia (NH_3) to form inorganic nitrate aerosols (R6) (Zhang et al., 2024a). Adaptationally, OH radicals can degrade organic volatile organic compounds (VOCs), leading to the formation of RO_2 radicals (R7) that further contribute to the generation of secondary organic aerosols (SOA) (Wang et al., 2017). Concurrently, RO_2 can react with NO to produce NO_2 (R8), a reaction that reduces ozone (O_3) titration (R9) while providing NO_2 for the subsequent formation of O_3 through reactions R10 and R11.

$$HONO \rightarrow OH + NO \quad (R4)$$

$$OH + NO_2 \rightarrow HNO_3 \quad (R5)$$

$$HNO_3 + NH_3 \rightarrow NH_4NO_3 \quad (R6)$$

$$VOC + OH \rightarrow RO_2 + H_2O \quad (R7)$$

$$RO_2 + NO \rightarrow RO + NO_2 \quad (R8)$$

$$O_3 + NO \rightarrow O_2 + NO_2 \quad (R9)$$

$$NO_2 + h\nu \rightarrow O^3P + NO \quad (R10)$$

$$O^3P + O_2 \rightarrow O_3 \quad (R11)$$

Over the past decade, there has been a notable increase in research interests about the topics related to HONO due to its critical potential to induce secondary air pollution in China (Jiang et al., 2024; Xue, 2022). The majority of previous studies have focused on elucidating the mechanisms of HONO formation and its associated environmental impacts, especially in city clusters of China that frequently experience severe air pollution (Fu et al., 2019; Li et al., 2022; Ran et al., 2024; Zhang et al., 2021, 2022c, 2023). For instance, Fu et al. (2019) demonstrated that HONO can intensify O_3

https://doi.org/10.5194/egusphere-2025-2630
Preprint. Discussion started: 8 August 2025

pollution by up to 24 ppbv during haze events in the Pearl River Delta (PRD) region of China. Meanwhile, Zhang et al. (2021) concluded that the enhanced AOC conditions contributed by HONO chemistry increased secondary aerosol concentrations by 18–51% in the North China Plain (NCP). We also previously investigated the role of HONO in the synergistic evolution of particulate matter and O_3 compound air pollution over the Yangtze River Delta (YRD) region (Zhang et al., 2024b).

Observational studies conducted in polluted urban areas indicated that lower concentrations of HONO typically occurred around noon (Fu et al., 2019; Song et al., 2023; Wang et al., 2025; Zhang et al., 2021). However, a recent in-situ measurement study in coastal regions revealed an inverse diurnal variation pattern of HONO concentrations. Specifically, Zhong et al. (2023) reported that their measurement campaign in Qingdao, a coastal city adjacent to the Yellow Sea, identified an unexpected diurnal peak in HONO concentrations at 12:00 local time (UTC+8). This suggests that oceanic contributions may affect the diurnal formation of HONO on land. But the mechanisms of HONO formation in coastal regions are not well understood by existing studies. Moreover, the maritime industry is an essential source of oceanic emissions. A previous study confirmed that shipping activities can emit substantial amounts of NO_x (Liu et al., 2016). As NO_x is a key precursor of HONO, shipping emissions can considerably impact the subsequent chemical production of HONO on land near the ocean (Dai and Wang, 2021). Furthermore, HONO emissions have been acknowledged as a result of shipping activities (Ke et al., 2025; Sun et al., 2020). Nevertheless, the contribution of shipping emissions to HONO formation in coastal areas has yet to be quantitatively assessed.

This study aims to investigate the mechanisms of HONO formation and its impact on the enhancement of OH radicals and O_3 in Fujian, a representative coastal region in southeastern China. To this end, we first conducted a one-month field measurement to characterize the levels and diurnal patterns of coastal HONO concentrations (see Section 3.1). We then employed the Weather Research and Forecasting model coupled with Chemistry (WRF-Chem) to reproduce the observed variations in HONO and performed a chemical budget analysis of HONO using process analysis techniques (refer to Sections 3.2 and 3.3). The model utilized in this study is based on our previous updates of the multiple HONO sources (Zhang et al., 2024b). In Section 3.3, we conducted a sensitivity experiment by zeroing out shipping emissions to clarify the influence of maritime activities on coastal HONO formation. Subsequently, we assessed the contribution of HONO photolysis to elevated coastal OH radicals and O_3 concentrations, as described in Section 3.4. The relevant uncertainties in the model were discussed in Section 3.5. Overall, this study comprehensively integrated field measurements and three-dimensional (3D) numerical simulations to improve our understanding of HONO formation mechanisms and its environmental implications for ambient oxidants in coastal regions of southeastern China.

https://doi.org/10.5194/egusphere-2025-2630
Preprint. Discussion started: 8 August 2025

2 Data and Methods

2.1 Field Measurements and Instrument

The in-situ measurement was conducted during the period from 1 to 31 May of 2024. The sampling location was the Dongzhen Reservoir (DZSK, 118.98°E, 25.48°N), which was categorized as a suburban site in Putian. The DZSK site was 6 km from downtown of Putian and approximately 25 km from the Taiwan Strait. The geographical location of DZSK is shown in Figure 1. Hourly HONO concentrations were measured using a long-path absorption photometer (LOPAP). The other two gaseous air pollutants, NO_2 and O_3, were measured using a commercial chemiluminescence instrument (Thermo Fisher Scientific 17i and 49i). Air temperature and relative humidity were monitored by a micro automatic weather station (LUFFT). Ultraviolet radiation (UV-A) was simultaneously observed with a solar radiation instrument (Kipp & Zonen). As records of the hourly wind field and precipitation were missing for the study period, observations were obtained from alternative sources. For wind speed and direction, we collected the U10 and V10 variables, representing wind components at 10 meters, from the ERA5 reanalysis dataset archived on the European Centre for Medium-Range Weather Forecasts (ECMWF) platform. Additionally, we obtained the precipitation data observed by the regional meteorological station in Putian (119.00°E, 25.44°N) for further analysis.

2.2 Regional Chemical Transport Model

WRF-Chem is one of the most widely used regional chemical transport models in atmospheric chemistry modeling (Zhang et al., 2024a). It can simulate the evolution of ambient trace gases and aerosols with fully coupled meteorology-chemistry feedback (Grell et al., 2005). This study used WRF-Chem (version 4.1.5) to explore coastal HONO formation and the associated environmental influences. To align with the measurement campaign, the model was run from 26 April to 31 May in 2024. The first five days were reserved for spin-up and were excluded from the data analysis. The entire simulation was conducted in a seven-day loop cycle to avoid systemic biases. The modeling domain focused on the southeastern coastal region of China (Figure 1), with a grid spacing of 10 km. Fujian Province is highlighted in a blue dashed box in Figure 1a. The coastal regions of Fujian consist of plains with a terrain elevation of less than 500 meter. Central Fujian is occupied by longitudinal mountains. This study focuses on six coastal cities for further discussion. As shown in Figure 2b, these cities are, from north to south: Ningde (ND), Fuzhou (FZ), Putian (PT), Quanzhou (QZ), Xiamen (XM), and Zhangzhou (ZZ). The observational site DZSK is located in the suburbs of Putian. In addition, 30 vertical layers were set up, extending from the ground surface to a height of 50 hPa.

The initial and lateral meteorological input conditions were derived from the final (FNL) global reanalysis dataset of the National Oceanic and Atmospheric Administration (NOAA). We also utilized four-dimensional data assimilation (FDDA)

https://doi.org/10.5194/egusphere-2025-2630
Preprint. Discussion started: 8 August 2025

to constrain gridded surface and upper atmospheric parameters with extra weather observational datasets. Continental anthropogenic emissions were obtained from the Multi-resolution Emission Inventory for China (MEIC version 1.4) (Li et al., 2017; Zheng et al., 2018). Shipping emissions were obtained from the Shipping Emission Inventory Model (SEIM), which was developed by Tsinghua University (Liu et al., 2016). Figure S1 illustrates the spatial distribution pattern of continental and oceanic shipping emissions within the modeling domain. Biogenic emissions were calculated online using the Model of Emissions of Gases and Aerosols from Nature (MEGAN, version 2.0.6) (Guenther et al., 2006). Furthermore, this study adopted various parameterizations to predict sub-grid atmospheric physical and chemical processes. The detailed information was compiled in Table 1. The Statewide Air Pollution Research Center (SAPRC99) mechanism (Carter, 2000) and the Model for Simulating Aerosol Interactions and Chemistry (MOSAIC) (Zaveri et al., 2008) were selected for gas-phase and aerosol chemistry simulations, respectively. The Fast-J module was chosen to calculate the photolytic rates of trace gases (Wild et al., 2000).

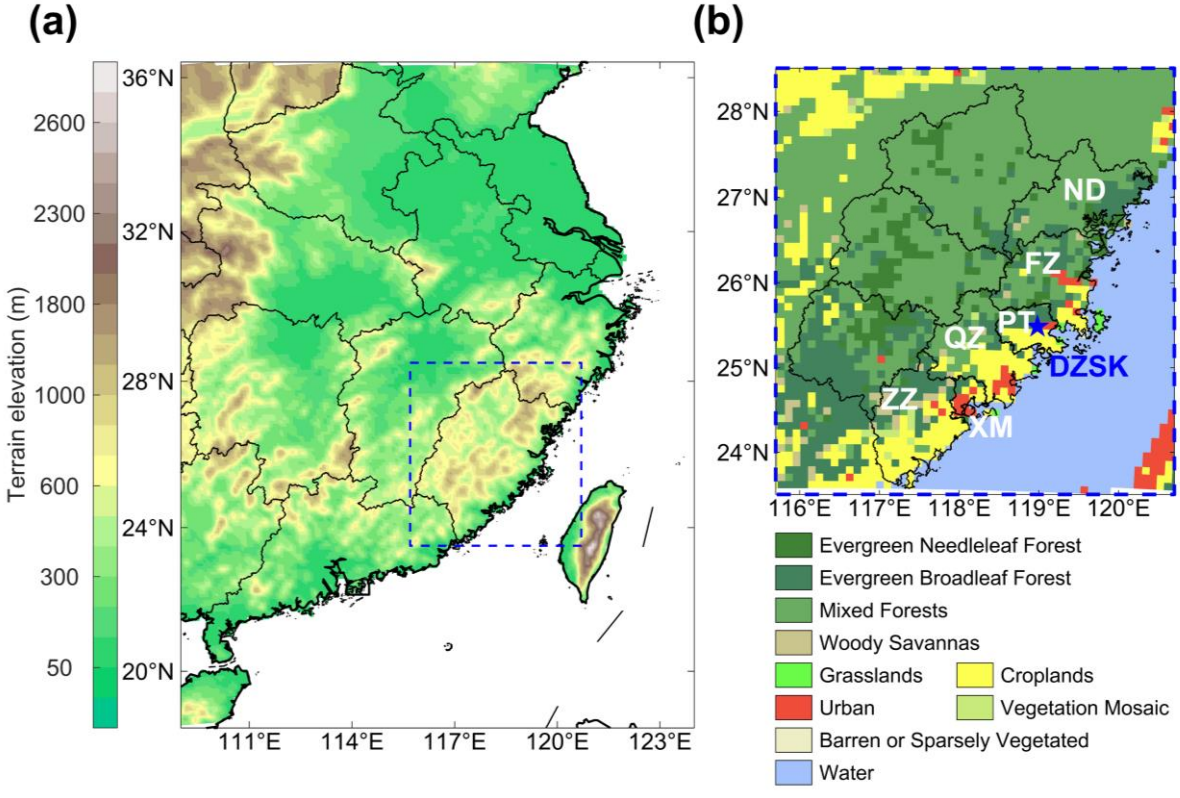

Figure 1. Design of the WRF-Chem modeling domain used in this study. Panel (a) depicts the terrain elevation of the modeling domain. Panel (b) illustrates the land use information in Fujian Province. The DZSK site (blue pentagram) and the six coastal cities (white bold font) are also marked in Panel (b).

https://doi.org/10.5194/egusphere-2025-2630
Preprint. Discussion started: 8 August 2025

Table 1. List of WRF-Chem modeling configurations.

	Parameter	Configuration
Time setup	Simulation duration	From 26th Apr to 31st May, 2024
	Spin-up period	5 days
Domain setup	Grid number	180 × 210
	Domain center	116.2 °E, 27.8 °N
	Horizontal resolution	10 km × 10 km
	Vertical configuration	30 layers from surface to 50 hPa height
	Projection	Lambert conformal
Physical parameterization	Microphysics	Lin (Lin et al., 1983)
	Long-wave radiation	RRTMG (Iacono et al., 2008)
	Short-wave radiation	RRTMG (Iacono et al., 2008)
	Surface layer	MM5 Monin-Obukhov (Jiménez et al., 2012)
	Land surface	Noah (Chen and Dudhia, 2001)
	Boundary layer	YSU (Hong et al., 2006)
	Cumulus	Grell 3D (Grell and Dévényi, 2002)
Chemical parameterization	Gas-phase reactions	SAPRC99 (Carter, 2000)
	Aerosol processes	MOSAIC (Zaveri et al., 2008)
	Photolysis	Fast-J (Wild et al., 2000)

2.3 HONO Source Updates and Process Analyses

In the original WRF-Chem model, the default source of HONO formation is the homogeneous reaction between NO and OH radicals. In a previous study, we incorporated multiple additional HONO sources into the WRF-Chem model (Zhang et al., 2024b), including direct emissions from fuel combustion processes, photo- and dark-oxidation of NO_x, light-enhanced heterogeneous uptake of NO_2 on the ground and aerosol surfaces, and photolysis of particulate nitrate aerosols. Updates to the chemical parameterizations of the HONO sources are summarized in Table 2. The heterogeneous uptake of NO_2 by ground and aerosol surfaces was light-dependent. We assumed that the nighttime uptake coefficients (γ) on the ground and aerosol surfaces were 8×10^{-6} and 4×10^{-6}, respectively (Zhang et al., 2021). During the daytime, the enhanced sunlight condition could increase the γ value to a maximum of 1×10^{-3} for the aerosol surface and 6×10^{-5} for the ground surface. For the remaining daylight hours, we applied a dynamic linear scaling formula adjusted by solar radiation intensity, as presented by Song et al. (2023). In addition, two key parameters have been updated in this study to more accurately represent the HONO formation rate in typical coastal regions. The first parameter is the ratio of HONO to NO_x ($HONO/NO_x$), which reflects emission intensity. Here, we utilized the value of 1.45% proposed by Hu et al. (2022) based on long-term in situ measurements in Xiamen, Fujian. This value more accurately represents direct HONO emissions from local fuel combustion. Simultaneously, we estimated HONO emissions from the shipping sector using the same ratio. Secondly, we set the photolysis frequency of nitrate aerosols (J_{no3-}) to 120 times that of gaseous HNO_3 (Fu et al., 2019; Ye et al., 2016, 2017).

https://doi.org/10.5194/egusphere-2025-2630
Preprint. Discussion started: 8 August 2025

Table 2. Chemical parameterizations of HONO sources in the revised WRF-Chem model.

Pathway	Parametrization	Descriptions
Direct Emissions	$E_{HONO} = \frac{HONO}{NO_x} \times E_{NO_x}$	E_{HONO} and E_{NOx} are emissions of HONO and NO_x. $HONO/NO_x$ = 1.45% (Hu et al., 2022)
Heterogeneous uptake of NO_2 by ground surface	$k_g = \frac{1}{8} \times v_{NO_2} \times \frac{S}{V} \times \gamma$	k_g, V_{NO2}, S/V, and γ are uptake reaction rate of NO_2 by the ground surface (s^{-1}), average molecular velocity (cm s^{-1}), ground surface area density (cm^2 cm^{-3}), and the unitless uptake coefficient (Zhang et al., 2024b).
Heterogeneous uptake of NO_2 by aerosol surface	$k_a = \frac{1}{4} \times v_{NO_2} \times \frac{S}{V} \times \gamma$	k_a, V_{NO2}, S/V, and γ are uptake reaction rate of NO_2 by the aerosol surface (s^{-1}), average molecular velocity (cm s^{-1}), aerosol surface area density (cm^2 cm^{-3}), and the unitless uptake coefficient (Zhang et al., 2024b).
Photolysis of nitrate aerosols	$J_{NO3^-} = 120 \times J_{HNO3}$	J_{NO3^-} and J_{HNO3} are the photolysis frequencies of nitrate aerosols and gaseous HNO_3 (Fu et al., 2019).
Photo- and dark-oxidation of NO_x	$HNO_3 + NO \rightarrow NO_2 + HONO$ $NO_3 + NO \rightarrow 1.98\ NO_2 + 0.02\ HONO$	Laboratory-based reaction kinetics from Song et al. (2023).

We used a source-oriented method (SOM) to determine the proportion of HONO production and consumption processes contributed by each source. A detailed description of the SOM diagnostic module can be found in Zhang et al. (2024b). In the SOM analysis, seven variables were configured to trace the formation process of HONO. These variables included the homogeneous reaction between NO and OH (NO+OH), NO_x photo-oxidation, NO_x dark-oxidation, primary emissions, the heterogeneous uptake of NO_2 by aerosols (Hetero-aerosol), the heterogeneous uptake of NO_2 on the ground surface (Hetero-land) and the photolysis of nitrate aerosols (Nitrate-photolysis). The first three sources are categorized as gaseous reaction, while the latter three are categorized as surface reactions. We also quantified two HONO chemical sink pathways: photodissociation of HONO (HONO+hv) as well as OH-oxidation removal (HONO+OH). Similarly, we also set up the SOM analysis to investigate the formation of OH radicals. Five formation pathways were identified, including the gas-phase reaction between HO_2 and NO (HO_2+OH), the reaction between atomic oxygen (O^1D) and H_2O (O^1D+H_2O) initiated by O_3 photolysis (O_3+hv → O^1D+O_2), photolysis of HONO (HONO+hv), photolysis of hydrogen peroxide (H_2O_2+hv), and ozonolysis of VOCs (O_3+VOCs). All of these chemical reactions are primary sources of OH radical formation except HO_2+OH, which is generally considered as a secondary conversion (Xue et al., 2025).

https://doi.org/10.5194/egusphere-2025-2630
Preprint. Discussion started: 8 August 2025

2.4 Sensitivity Experiment Designs

Our study also conducted sensitivity experiments to quantify the contribution of oceanic shipping emissions to the formation of HONO in coastal areas, and the contribution of HONO chemistry to the enhancement of ambient OH radicals and O_3. In total, three simulation cases were run, using the same meteorological initial and lateral conditions and continental anthropogenic and biogenic emissions. As listed in Table S1, the first case was the BASE case, which considered oceanic shipping emissions but did not include the updated HONO sources. The REV case included both oceanic shipping emissions and the updated HONO formation pathways. The "Noship" case denotes a simulation that used an improved HONO source representation but excluded oceanic shipping emissions. By comparing the BASE case (or Noship) with the REV case, we estimated the respective contribution of the updated chemical sources and shipping emissions to HONO formation.

3 Results and Discussions

3.1 Overview of Field Observations

Figure 2 shows hourly observations of air pollutants and meteorological parameters at the DZSK site from 1 to 31 May 2024. Generally, HONO concentrations ranged from 0.01 to 1.11 ppbv, with an average of 0.23 ppbv. We compared the HONO measurements at the DZSK site with in situ observations collected from previous studies in China. Table S2 presents a dataset of HONO measurements from 43 studies conducted between 2008 and 2025. It can be concluded that observational studies were intensively carried out in urban areas of the NCP region, particularly in Beijing, where recorded HONO concentrations frequently exceeded 1 ppbv. These higher HONO levels were attributed to abundant NO_x emissions. By contrast, HONO concentrations were found significantly lower in remote regions. For instance, HONO concentrations ranging from 0.13 to 0.15 ppbv were measured at the summit of Mt. Tai (Jiang et al., 2020; Xue et al., 2022). Studies of coastal regions witnessed HONO concentrations of around 0.50 ppbv (Hu et al., 2022; Zhong et al., 2023). Overall, the HONO levels measured at the DZSK site were much lower than those reported by previous measurements in China. The mean NO_2 concentration during the study period was 6.3 μg m^{-3}, due to low NO_x emissions in the suburban, which probably contributed to the low HONO concentrations. Meanwhile, the average wind speed was 2.1 m s^{-1}, providing a favourable diffusion condition for air pollutants. The prevailing wind direction at the DZSK site was from the northeast, implying a potential contribution from oceanic shipping emissions.

Figure S2 exhibits the diurnal variations of gaseous air pollutants and meteorological parameters. On non-rainy days, air temperature and solar radiation were higher, with an apparent peak occurring around midday. Substantial sunlight

https://doi.org/10.5194/egusphere-2025-2630
Preprint. Discussion started: 8 August 2025

accelerated the photochemical production of air pollutants such as O_3. Consequently, concentrations of air pollutants were obviously higher on non-rainy days than on rainy days. At the same time, precipitation also led to the wet deposition of air pollutants. To avoid the influence of precipitation, we focused on the diurnal variation pattern of HONO concentrations excluding rainy days. The maximum hourly HONO concentration at the DZSK site occurred at 14:00 on non-rainy days, peaking at 0.38 ppbv. This phenomenon is contrary to the diurnal variations of HONO observed in previous inland measurements. According to Wang et al. (2025), HONO concentrations in inland urban and rural areas typically displayed the minimum in the afternoon. Despite the decrease in air temperature and radiation after 14:00, the O_3 concentration increased until it reached a daily maximum of 125 μg m^{-3} at 16:00. To explore the mechanisms of HONO formation in coastal regions, especially the diurnal peak during the daytime, our study conducted SOM process analyses in the subsequent sections. The potential contribution of shipping emissions to coastal HONO formation was also quantified using sensitivity experiments.

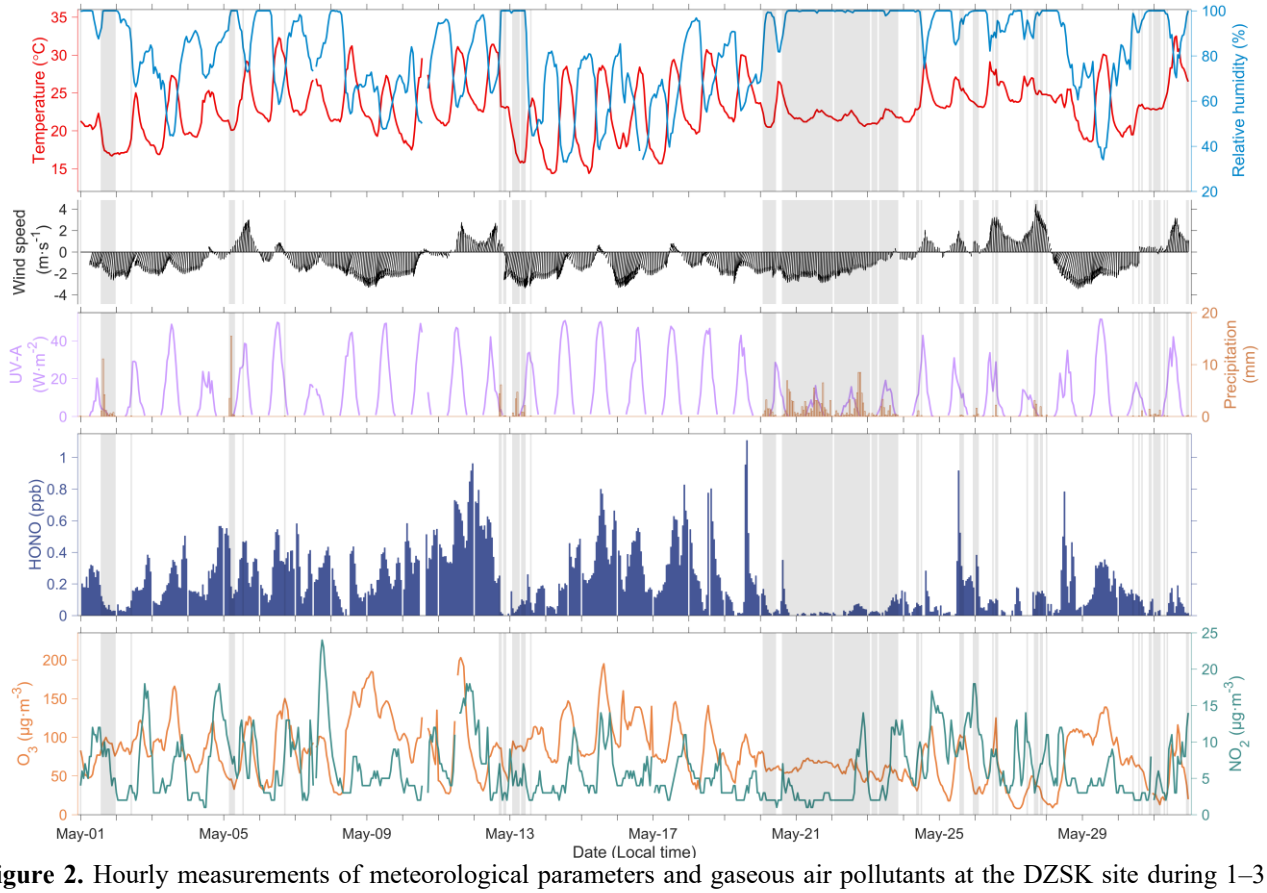

Figure 2. Hourly measurements of meteorological parameters and gaseous air pollutants at the DZSK site during 1–31 May 2024. The shaded areas stand for the period of precipitation.

https://doi.org/10.5194/egusphere-2025-2630
Preprint. Discussion started: 8 August 2025

3.2 Evaluations of the Numerical Model

First, we conducted a model evaluation based on measurements at the DZSK site. Figure 3 demonstrates a comparison between the simulated and observed HONO concentrations. The BASE simulation failed to capture the magnitude and temporal variations of HONO concentrations at the DZSK site. Including multiple HONO formation pathways greatly improved the model performance of HONO (Figure 3a). The monthly mean HONO concentration increased from 0.03 ppbv (BASE) to 0.25 ppbv (REV). We then applied three statistical metrics to reveal improvements in HONO modeling. The calculation of validation indicators has been elucidated in our previous modeling studies (Zhang et al., 2024b). As summarized in Table 3, the index of agreement (IOA, varies from 0 to 1) for predicting hourly HONO concentrations increased from 0.62 (BASE) to 0.69 (REV). Simultaneously, the normalized mean bias (NMB, varies from –∞ to +∞) and the root mean square error (RMSE, varies from 0 to +∞) considerably decreased by 91% and 21%, respectively. While the revised model reasonably reproduced the observed temporal variations in HONO concentrations during the study period, an underestimation existed on 16–18 May, suggesting a potential omission of HONO sources. Additionally, the WRF-Chem model overestimated low HONO concentrations during 21–24 May, when there was continuous precipitation (Figure 2). Simulations including the updated HONO sources more accurately represented the diurnal variation pattern of HONO concentrations. Figure 3c illustrates that the REV case successfully captured the higher HONO concentrations observed around noon. The Pearson's correlation coefficient (R) between the measurements and simulations increased from 0.657 (BASE) to 0.763 (REV).

Table 3. Statistical metrics of evaluating HONO simulations.

	Mean observation (ppbv)	Mean simulation (ppbv)	IOA	NMB	RMSE (ppbv)
BASE	0.23	0.03	0.62	– 86%	0.28
REV	0.23	0.25	0.69	+ 8%	0.22

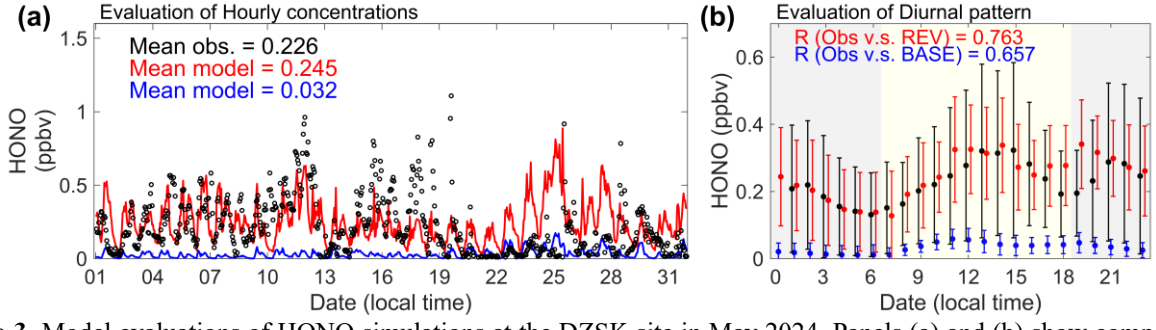

Figure 3. Model evaluations of HONO simulations at the DZSK site in May 2024. Panels (a) and (b) show comparisons between observations and simulations of hourly and diurnal HONO concentrations, respectively. The red and blue fonts represent the REV and BASE modeling cases, respectively. The lower and upper limits in panel (b) indicate the mean ± standard deviation (σ).

https://doi.org/10.5194/egusphere-2025-2630
Preprint. Discussion started: 8 August 2025

The model performance for important precursors and products of HONO chemistry, NO_2 and O_3, were improved as well. As illustrated in Figure 4a and 4c, the diurnal variations in the simulated NO_2 and O_3 concentrations by REV were more consistent with the observed values. The diurnal Pearson's correlation coefficients between measurements and simulations for NO_2 and O_3 increased by 5% and 3%, respectively. At the same time, underestimation of O_3 concentrations in the original model was effectively reduced. The daily maximum O_3 concentration in the revised version (REV) was much closer to the observed value than in the BASE simulation. The estimated maximum daily average 8-hour (MDA-8) concentration of O_3 increased from 62.9 μg m^{-3} (BASE) to 85.6 μg m^{-3} (REV), with an observed value of 103.0 μg m^{-3} (Figure 4d). Accurately characterizing the HONO chemical budget can therefore improve the simulation of O_3 concentrations in 3D chemical transport models.

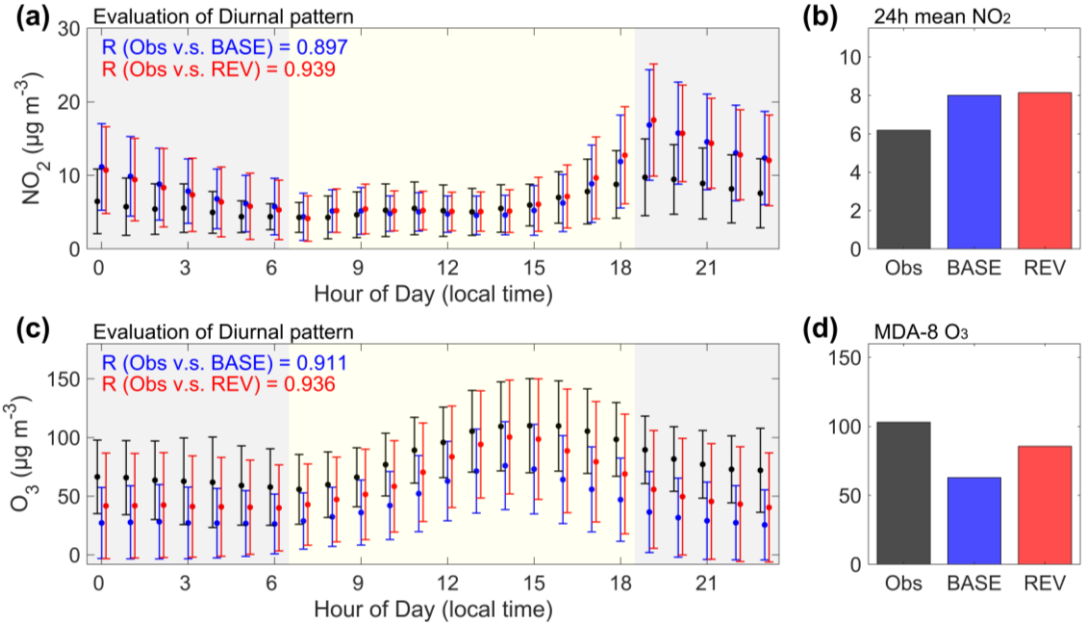

Figure 4. The same as Figure 3b, but for diurnal variations of NO_2 and O_3 concentrations.

3.3 Analyses of HONO Formation Mechanisms

3.3.1 Spatio-temporal Characteristics

This study used SOM process analysis to elucidate the mechanisms of HONO formation in Fujian's coastal regions. The analysis focused on the regional average from six coastal cities, as depicted in Figure 1. The diurnal variations in the chemical production and consumption rates of HONO are presented in Figure 5a. The maximum HONO production rate of over 1.30 ppbv h^{-1} occurred during the midday hours (11:00 to 14:00), due to the intensified formation pathways. The

https://doi.org/10.5194/egusphere-2025-2630
Preprint. Discussion started: 8 August 2025

HONO consumption rates were primarily influenced by self-photolysis (HONO+hv) and exhibited a diurnal pattern similar to that of the production rates. The average HONO production rate during the daytime (7:00 to 18:00) was found to be 0.97 ppbv h^{-1} (Figure 5b). The SOM analysis revealed that gas-phase and surface reactions contributed equally to daytime HONO formation, accounting for 45% each. Specifically, the heterogeneous uptake of NO_2 on the ground surface and photo-oxidation of NO_x emerged as the two principal contributors to HONO formation in coastal regions, with an aggregate contribution of 64%. In descending order, other sources contributed 16% (NO+OH), 10% (primary emissions), 8% (nitrate-photolysis), 2% (hetero-aerosol), and less than 1% (NO_x dark-oxidation) to daytime HONO formation. Although the heterogeneous uptake of NO_2 on the ground surface was identified as the predominant pathway, its relative importance evidently declined from morning to afternoon (Figure 5a). This decrease could be attributed to the growing influence of nitrate photolysis, NO+OH, and NO_x photo-oxidation. The mean nocturnal HONO production rate dropped to 0.12 ppbv h^{-1}, reflecting a substantial decline in the intensity of oxidation-related HONO formation pathways (Figure 5b). At the same time, HONO consumption rates approached zero at night due to the cessation of photochemical loss mechanisms. Overall, the heterogeneous NO_2 uptake on the ground surface remained the dominant source for nighttime HONO production, accounting for 48%. In the meantime, the contribution of direct emissions to nocturnal HONO production significantly increased to 17%.

The mechanisms of HONO formation also proposed spatial heterogeneity. Our study examined HONO formation pathways across different land surfaces, such as forests, grasslands, farmlands, and urban areas (see Table S3). Figure 1b illustrates the spatial distribution of land use information within the study region. In forested areas, SOM analysis indicated that heterogeneous uptake of NO_2 by the ground surface accounted for 45% of HONO production. This phenomenon is likely linked to the higher density of reactive surface area resulting from the larger leaf area index (LAI) of forested areas (Zhang et al., 2016). In urban areas, however, high NO_x levels could facilitate greater HONO production through gas-phase reactions involving NO_x, particularly NO_x photo-oxidation and NO+OH, which contributed 36% and 21%, respectively. The absolute HONO production rates from these two NO_x-related reactions in urban areas were approximately four times higher than in forests. Direct emissions also contributed significantly to HONO formation (23%) due to intensive NO_x emissions in urban areas. Since two-thirds of the coastal areas are covered by forests, the regional average contribution of NO_2 heterogeneous uptake on the ground surface exceeded that of any NO_x-related gas-phase oxidation reaction or direct emissions.

Previous investigations have indicated that light-enhanced heterogeneous uptake of NO_2 on the ground surface is the dominant source of HONO formation in inland regions (Zhang et al., 2024b). Our diagnostic results in the coastal regions of Fujian support this finding. However, the specific contribution in Fujian (35–48%) was obviously lower than that observed in inland areas (42–86%). Similarly, the contribution from the heterogeneous NO_2 uptake on aerosol surfaces

https://doi.org/10.5194/egusphere-2025-2630
Preprint. Discussion started: 8 August 2025

(1–2%) was lower than that reported for inland areas (3–20%), because of lower particle concentrations in coastal regions. Moreover, the present study pointed out a greater contribution to HONO formation from NO_x-related gas-phase oxidation reactions than was found in previous studies.

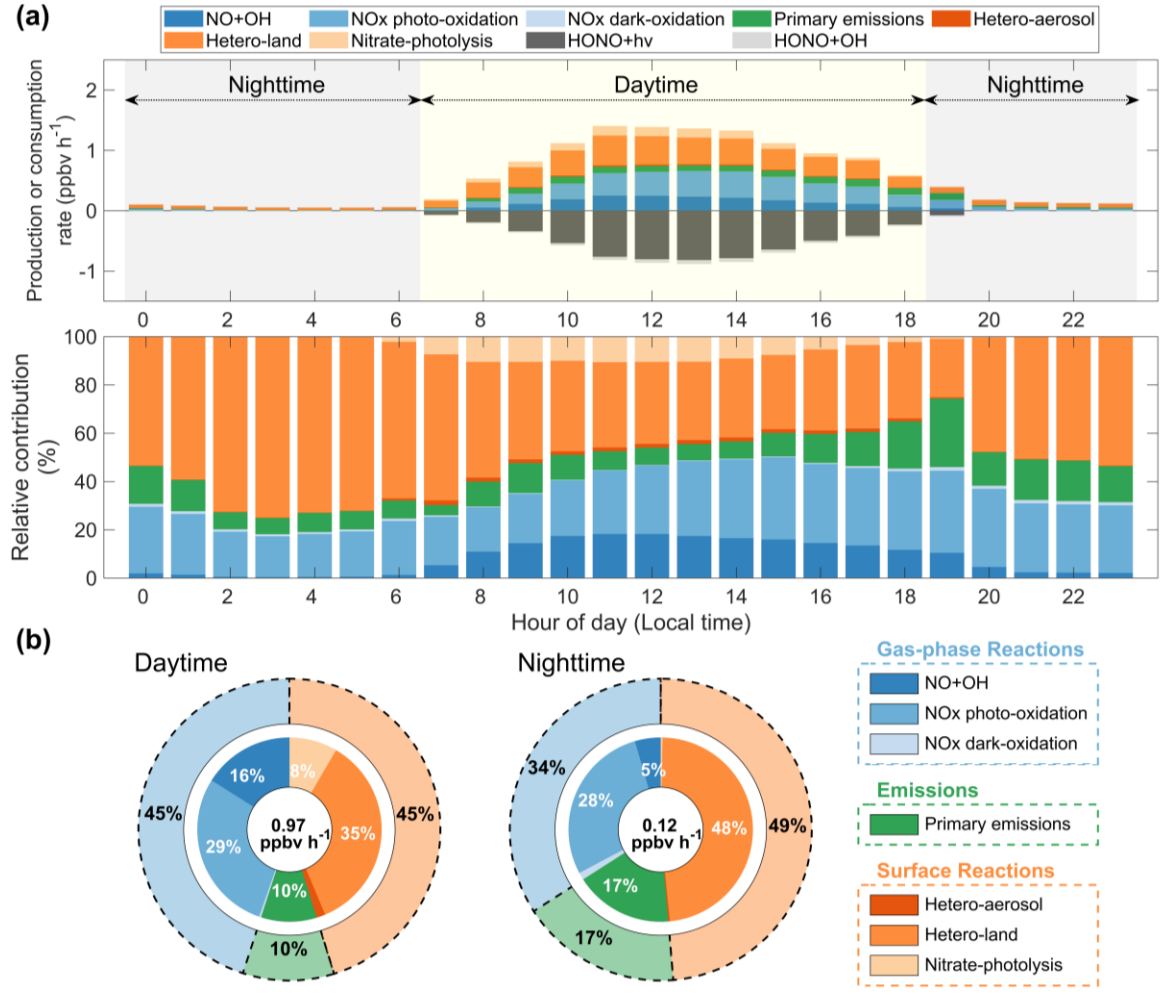

Figure 5. Attribution of mechanisms of HONO formation in coastal Fujian in May 2024. Panel (a) shows the diurnal variations in the absolute and relative contributions of seven production and two consumption reactions to the HONO chemical budget. Panel (b) illustrates the contribution of the seven production reactions to daytime and nighttime HONO formation during the study period. The total production rates are labelled in the middle of the pie charts.

3.3.2 Impact of Shipping Emissions

Furthermore, we conducted sensitivity experiments to evaluate the potential impact of shipping emissions on HONO formation in coastal regions. Figure 6 demonstrates the spatial distribution of NO_x, NO_3^-, and HONO concentrations in

https://doi.org/10.5194/egusphere-2025-2630
Preprint. Discussion started: 8 August 2025

coastal regions that can be attributed to shipping emissions. As NO_x is the most important precursor for HONO formation, we first examined the influence of shipping emissions on coastal NO_x concentrations. The results indicated that shipping emissions caused a net increase of 0.68 ppbv in NO_x levels across the coastal regions of Fujian, with a clear decrease in gradient from the ocean towards inland areas. It is revealed that shipping emissions contributed 17% to coastal NO_x concentrations, with a higher contribution in the northern regions than in the middle urban areas. The subsequent rise in NO_x concentrations led to an increase in nitrate aerosol concentrations, which probably facilitated HONO formation. Spatially, shipping emissions induced a net elevation in the average NO_3^- concentration of 0.52 μg m^{-3}, accounting for approximately 33% of the total. The spatial distribution of nitrate aerosol concentrations differed from that of NO_x, with higher levels concentrated mainly in areas with intensive NH_3 emissions. Consequently, HONO levels in the coastal regions of Fujian increased by 36 pptv due to increased precursor concentrations resulting from shipping emissions, representing an 18% relative contribution. Similar to the NO_x spatial distribution pattern, shipping emissions promoted higher HONO levels in the northern areas of the study region.

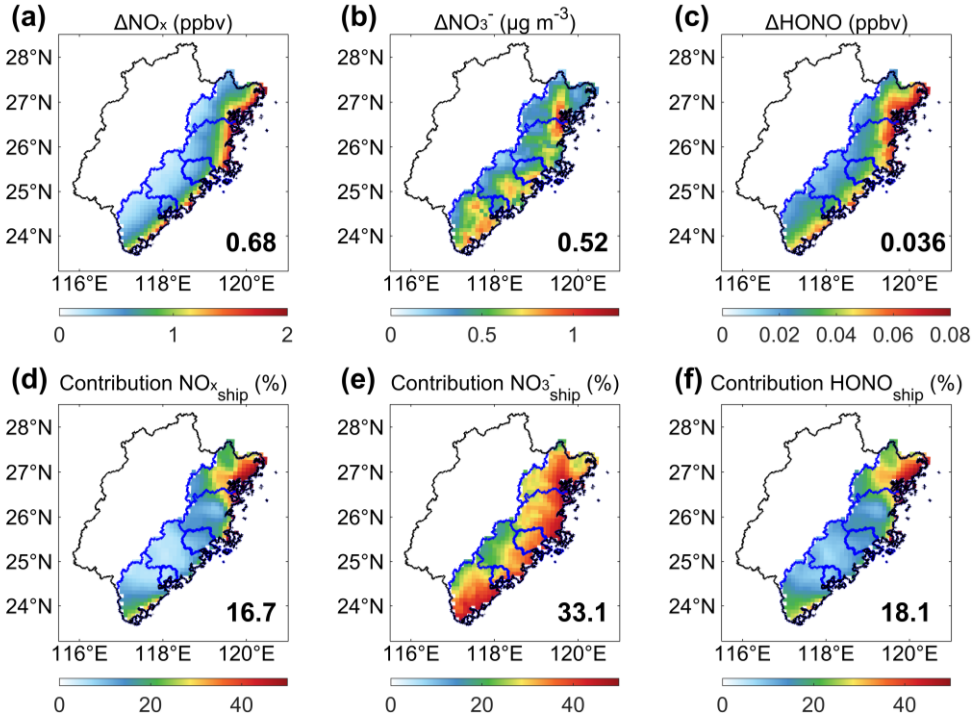

Figure 6. The simulated regional mean effect of shipping emissions on the concentrations of HONO and its precursors, including NO_x and NO_3^- aerosols, during the study period. Panels (a-c) show the absolute changes, while panels (d-f) represent the relative contributions from shipping emissions ($\frac{\text{REV-Noship}}{\text{REV}} \times 100\%$). The regional average values are marked in the bottom right-hand corner of each panel.

https://doi.org/10.5194/egusphere-2025-2630
Preprint. Discussion started: 8 August 2025

As illustrated in Figure S3, the simulated diurnal range of coastal NO_x concentrations attributed to shipping emissions was from 0.43 to 0.99 ppbv. This effect was more pronounced during the nighttime hours. Specifically, NO_x released from the shipping sector preferred to react with O_3 near the ocean surface. As depicted in Figure S4, the chemical production rates of O_3 during both daytime and nighttime were negative over coastal waters with substantial shipping emissions. This suggests that the transport of NO_x to coastal regions was probably inhibited. Meanwhile, the O_3 titration effect was more evident during the daytime than at night due to higher shipping emissions, meaning that shipping emissions contributed less to coastal NO_x during the daytime. Therefore, nitrate aerosols, the products of NO_x oxidation, exhibited the same diurnal variation pattern as NO_x with respect to contributions induced by shipping emissions (Figure S3). Despite the fact that NO_x and nitrate aerosols contributed by shipping emissions were relatively lower during the daytime, HONO production rates were higher, particularly around noon (Figure 7). This phenomenon could be attributed to light-dependent reactive pathways that efficiently increased HONO production rates in the presence of sunlight. The mean increased production rate of HONO in coastal regions resulting from shipping emissions during the daytime was 0.15 ppbv h^{-1}. Heterogeneous uptake of NO_2 on the ground surface, NO_x photo-oxidation, NO+OH, and nitrate photolysis accounted for 39%, 34%, 13%, and 12% of the total enhancement, respectively. In contrast, HONO production rates attributed to shipping emissions were much lower in the evening. However, due to the self-photolysis of HONO, the overall increase in coastal HONO concentrations caused by shipping emissions during the daytime (0.19 ppbv) was close to daytime levels (0.20 ppbv).

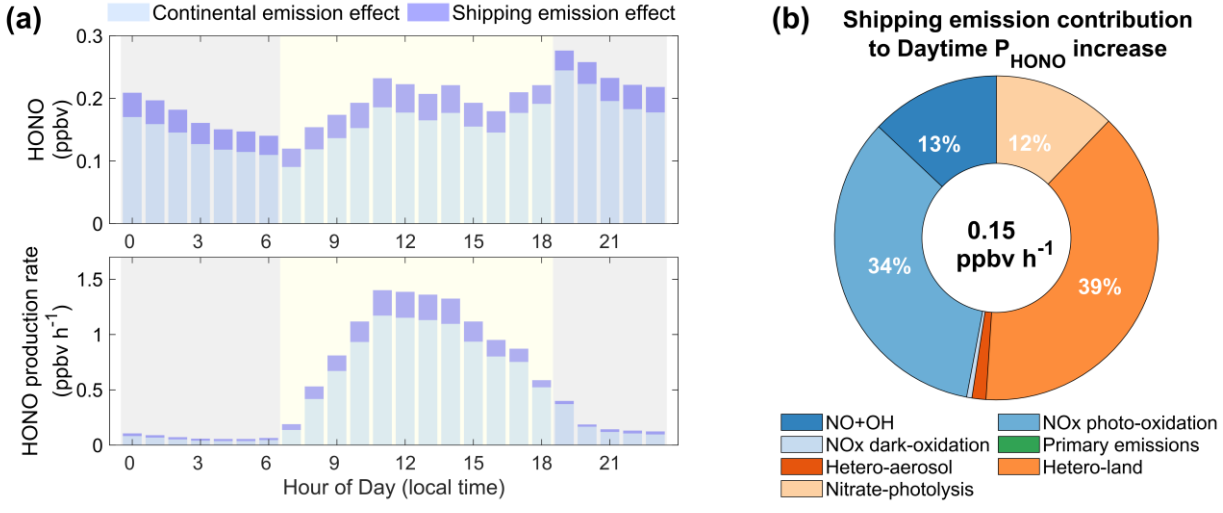

Figure 7. The simulated shipping emission contributions to concentrations and formation rates of HONO over the study region. Panel (a) shows the diurnal variations in the effects of continental and shipping emissions on HONO concentrations and formation rates. Panel (b) displays the contribution of shipping emissions to the daytime HONO production rate from different sources.

https://doi.org/10.5194/egusphere-2025-2630
Preprint. Discussion started: 8 August 2025

3.3.3 Attribution of Daytime High HONO Concentrations

We subsequently interpreted the causes of the high HONO levels in the coastal regions of Fujian. The predicted high HONO concentrations over the study region between 11:00 and 14:00 were attributed to a simultaneous increase in chemical production rates (see Figures 5a and 7a). The rapid conversion efficiency offset the effect of low NO_x and nitrate aerosol concentrations, leading to higher HONO production rates around noon. Meanwhile, the aggregate HONO production rate exceeded consumption rates resulting from self-photolysis and OH-oxidation reactions. This contributed to the accumulation of high HONO concentrations. Previous studies concluded that the daytime peak in HONO concentrations was possibly driven by nitrate photolysis (Hu et al., 2022; Wang et al., 2025). However, our attribution analysis inferred that nitrate photolysis was not the dominant factor. Even when an upper limit of the empirical photolysis frequency of nitrate aerosols ($120J_{HNO3}$) was applied (Fu et al., 2019; Zhang et al., 2022a), the low nitrate concentration of about 1.0 μg m^{-3} only accounted for less than 10% of the overall production rate during the daytime (Figure S3). This study suggests that heterogeneous NO_2 uptake on the ground surface and NO_x photo-oxidation were the main drivers of HONO formation around noon (11:00 to 14:00), contributing 30% and 34%, respectively. The high production rates of these two photo-chemical reactions could be attributed to the persistent abundant solar radiation in coastal areas. Analysis of the spatial distribution patterns of HONO formation mechanisms revealed that the NO_2 heterogeneous uptake reaction on the ground surface was more effective in forests, whereas the photo-oxidation of NO_x played a more important role in coastal urban areas (Table S3). In addition, HONO photolysis could release OH radicals, facilitating further photo-oxidation of NO_x, particularly at noon when the intensity of photochemistry reaches its diurnal peak. We also quantified the contribution of shipping emissions to coastal HONO levels in Figure 7. We found that 0.22 ppbv h^{-1} of the HONO production rate was attributable to shipping emissions around noon, resulting in a 20% increase in HONO concentrations. These results emphasize the importance of including shipping emissions in the HONO budget near coastal regions.

3.4 Contributions of HONO to Ambient Oxidants

3.4.1 Enhancement of OH Radicals

We assessed the role of HONO in OH formation over the coastal regions of Fujian utilizing the SOM process analysis. As illustrated in Figure 8, the OH production rates from four primary sources and one secondary source are presented. The total OH production rate peaked at 14:00, reaching a maximum value of 7.78 ppbv h^{-1} (Figure 8a). Conversely, OH production rates at night were significantly lower, remaining below 1 ppbv h^{-1}. The average daily OH production rate throughout the study period was calculated to be 2.61 ppbv h^{-1}. Notably, secondary conversion from the reaction between

https://doi.org/10.5194/egusphere-2025-2630
Preprint. Discussion started: 8 August 2025

HO_2 and NO was found to dominate OH production, contributing 68% of the total (Figure 8b). This fraction is consistent with the results of previous field measurement studies (Yang et al., 2021; Ye et al., 2023). Among primary sources identified, the reaction between O^1D and H_2O initiated by O_3 photolysis, and the photolysis of HONO emerged as two significant contributors to OH formation. These two pathways accounted for 15% and 10% of the daily OH production rate. Evidently, O^1D+H_2O and HONO+hv were more influential during daylight hours, with the combined contribution to the OH production rate peaking at 32% at 13:00.

Figure 8c illustrates the diurnal variations in the relative contributions to OH formation from four primary sources. Model results indicated that the contribution of HONO photolysis to OH formation was notably higher during morning hours. As O_3 concentrations increased, the reaction between O^1D and H_2O replaced HONO photolysis as the dominant source for OH formation. This phenomenon has been confirmed by previous observational studies conducted in coastal regions (Hu et al., 2022; Xue et al., 2025). The O^1D+H_2O reaction reached a maximum contribution of approximately 60% to OH formation at 14:00. After this peak, the production rates of all reactions decreased due to diminishing sunlight conditions. Generally, the average daytime production rate of OH in the coastal regions of Fujian was estimated to be 1.52 ppbv h^{-1}. The contributions of the O^1D+H_2O, HONO+hv, photolysis of H_2O_2, and ozonolysis of VOC the primary OH production rate were 51%, 34%, 8%, and 8%, respectively.

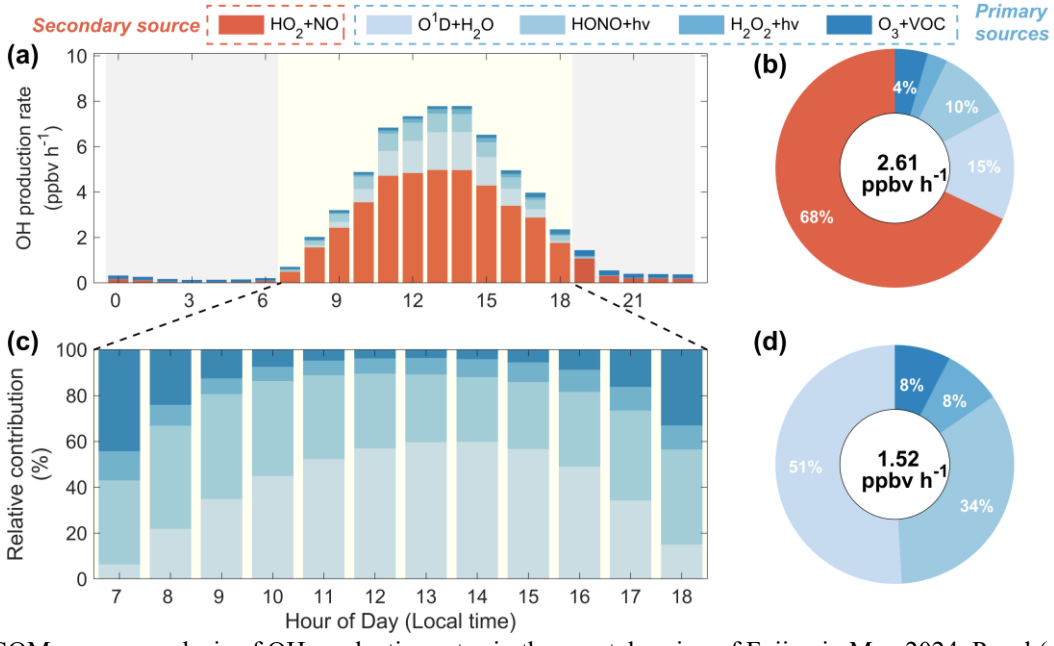

Figure 8. SOM process analysis of OH production rates in the coastal region of Fujian in May 2024. Panel (a) shows the diurnal variations of OH production rates from five sources. Panel (b) shows the relative contribution of each pathway. Panels (c-d) show the specific contribution of the four primary sources to OH formation during the daytime.

https://doi.org/10.5194/egusphere-2025-2630
Preprint. Discussion started: 8 August 2025

Through sensitivity experiments, we further elucidated the impact of HONO on OH concentrations. As shown in Figure 9a, the diurnal OH concentrations in the coastal regions of Fujian experienced a remarkable increase due to the improved representation of HONO sources in the WRF-Chem model. Compared to the BASE simulation, the average daytime concentration of OH radicals increased by 57%. Concurrently, the daily maximum OH concentration rose from 7.5×10^6 molecules cm^{-3} (BASE) to 12.1×10^6 molecules cm^{-3} (REV). This increase in OH concentration can be attributed to the alteration in OH production rate. The SOM process analysis indicated a 35% increase in the mean OH production rate.

By integrating sensitivity experiments with the SOM process analysis, we identified two principle factors that contributed to the enhancement of OH formation (Figure 9b). The first factor is the consequence of HONO photolysis, which increased the OH production rate by 0.40 ppbv h^{-1}. Due to the low HONO concentration in the BASE simulation, the contribution of the HONO photolysis to the OH production rate relatively surged by 378%. The second factor is the promotion of ambient AOC conditions. The increased OH levels then enhanced the formation of oxidative products, including HO_2 radicals, H_2O_2, and O_3. The rise in O_3 further accelerated the generation of O^1D atom. Consequently, the chemical reactions involving HO_2+NO, O^1D+H_2O, and H_2O_2+hv led to increases in the OH production rate of 0.63, 0.18, and 0.04 ppbv h^{-1}, with relative changes of 23%, 29%, and 53%, respectively. The contribution to OH production from the O_3+VOC reaction was negligible as this reaction was more efficient at night and inactive during the daytime. In conclusion, the direct increase in OH formation via HONO photolysis accounted for 32% of the overall effect attributed to HONO chemistry. The impact of the enhancement in the OH production rate contributed by the other four sources was twice that contributed by the photolysis of HONO (Figure 9c).

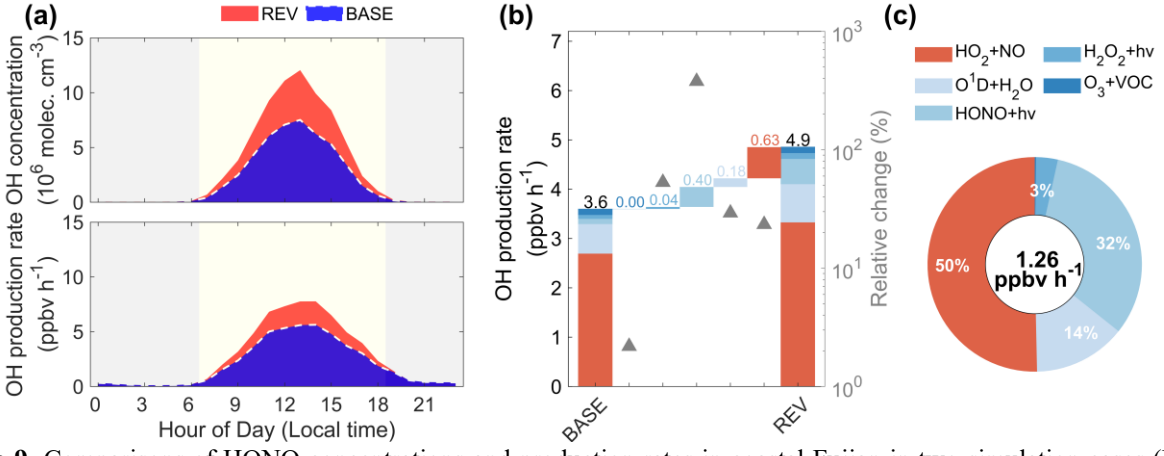

Figure 9. Comparisons of HONO concentrations and production rates in coastal Fujian in two simulation cases (BASE and REV). Panel (a) displays the diurnal variations in OH concentrations and production rates. Panel (b) shows the absolute and relative changes in daytime OH formation rates from five chemical sources by comparing the BASE and REV cases. The relative contribution of these sources to the enhancement of the OH production rate is exhibited in Panel (c), with the number of increased production rate labelled in the middle of the pie chart.

https://doi.org/10.5194/egusphere-2025-2630
Preprint. Discussion started: 8 August 2025

3.4.2 Enhancement of O_3 Concentration

The sensitivity experiment simultaneously assessed the impact of HONO chemistry on O_3 concentrations. As discussed in Section 3.2, the model evaluation of O_3 levels has revealed that the discrepancy between the BASE and REV cases arises from increased AOC conditions due to the updates of HONO representation. Switching from the BASE simulation to the REV simulation led to an increase in 24-hour average O_3 concentration by 9.2 ppbv at the DZSK site, representing a 43% relative increase. In the coastal regions of Fujian, the regional mean absolute enhancement of O_3 concentration was 9.9 ppbv, corresponding to a relative increase of 44%, comparable to the findings at DZSK. Moreover, we compared the simulated absolute and relative alternations in O_3 concentrations attributable to HONO chemistry with the results of sensitivity experiments utilizing 3D chemical transport models obtained from previous studies. The related comparisons are summarized in Table 4. Most of the referenced studies referenced were conducted in densely populated areas in eastern China. The compilation suggests that the absolute increase in O_3 concentration driven by HONO chemistry across most studies was approximately 10 ppbv and consistent with the value presented by this study. However, the relative enhancement of O_3 levels in this study (43–44%) was significantly higher than the range reported in previous studies (12–38%), exception for the outlier proposed by Fu et al. (2019). This discrepancy indicates a more pronounced catalytic impact of HONO on photochemical air pollution in coastal regions despite their comparatively lower concentrations of HONO.

Table 4. Compilation of contributions of HONO photolysis to enhancement of O_3 concentrations from previous studies.

Period	Region	Model	Absolute ΔO_3 (ppbv)	Relative ΔO_3 (%)	References
25–31 August 2011	Hong Kong	WRF-Chem	4.0	12	(Zhang et al., 2016)
26 June to 7 July 2014	East China	WRF-Chem	2.9–6.2	6–13	(Zhang et al., 2017)
4–8 January 2017	Heshan, PRD	CMAQ	24.0	70	(Fu et al., 2019)
22–31 July 2016	NCP	WRF-Chem	13.0	-	(Guo et al., 2020)
7–13 July 2013	YRD		14.7	-	
18–31 October 2015	PRD		10.7	-	
3 December 2015 to 14 January 2016	Xi'an	WRF-Chem	-	22	(Li et al., 2022)
1 March to 31 May 2016	NCP	WRF-Chem	7.9	17	(Zhang et al., 2022b)
1 July to 30 September 2016			8.9	16	
8–22 June 2017	NCP	WRF-Chem	26.1	38	(Song et al., 2023)
1–7 June 2017	NCP	WRF-Chem	6.9	16	(Ran et al., 2024)
8–13 June 2017			9.5	20	
14–21 June 2017			11.2	22	
24–27 March 2019	Nanjing, YRD	WRF-Chem	8.9	28	(Zhang et al., 2024b)
1–31 May 2024	DZSK	WRF-Chem	9.2	43	This study
	Coastal areas		9.9	44	

https://doi.org/10.5194/egusphere-2025-2630
Preprint. Discussion started: 8 August 2025

3.5 Uncertainties

There are several uncertainties in HONO simulations that should be discussed. Firstly, the heterogeneous uptake coefficients of NO_2 by solid surfaces and the photolysis frequency of nitrate are highly uncertain. The maximum uptake coefficient γ varies from 10^{-6} to 10^{-3} depending on sunlight conditions and surface properties (Zhang et al., 2024a). Previous studies have widely used maximum γ values of 1×10^{-3} for aerosol surfaces and 6×10^{-5} for the ground surface (Liu et al., 2019; Zhang et al., 2024b, 2021), demonstrating good robustness. Regarding the photolysis frequency, Zhang et al. (2022a) summarized that J_{no3-} is 1–3 orders of magnitude higher than J_{HNO3}. Our study adopted the median magnitude ($120J_{HNO3}$) inferred from aircraft-based measurements conducted in the marine boundary layer over the North Atlantic ocean (Ye et al., 2016), as this better represents coastal areas.

Secondly, we used an empirical $HONO/NO_x$ value of 1.45% to estimate the direct HONO emissions from the fuel combustion process. This value was derived from long-term in situ measurements in coastal regions and proposed by Hu et al. (2022). We applied this value to describe fresh HONO emissions from ships. However, Ke et al. (2025) have pointed out that the same ratio of HONO to NO_x may not be applicable to mobile sources, including mobile machinery, ships, and aircraft. Currently, there are no direct measurements of freshly emitted HONO from shipping. Therefore, further observations and experiments are required to constrain HONO emissions from ships.

Thirdly, the ocean surface may affect HONO formation in other ways. Zha et al. (2014) observed significant evidence suggesting that the ocean was a nonnegligible contributor to coastal HONO production. Consequently, Zhang et al. (2016) parameterized this reaction as heterogeneous uptake by the ocean surface in the WRF-Chem model using a simplified formula. Additionally, an observational study proposed that seawater could increase the solubility of HONO under certain conditions, indicating that the ocean surface could act as a sink for atmospheric HONO (Crilley et al., 2021; Wang et al., 2025). However, the source or sink effect of the ocean on HONO remains a controversial topic. Further studies on this theory and the relevant parameterization are needed in the future.

4 Conclusions

This study investigated the mechanisms of HONO chemical formation and its impact on the enhancement of ambient oxidants in coastal Fujian of southeastern China. Based on continuous in situ measurements over a one-month period at a suburban site, we found that the observed HONO showed an unexpected diurnal variation pattern with higher levels measured at noon, contrary to an obvious daytime minimum reported by extensive previous studies focusing on inland areas. Using a revised WRF-Chem model incorporating updates to multiple sources of HONO, including direct emissions, NO_2 heterogeneous uptake by solid surfaces, nitrate photolysis, and the photo- and dark-oxidation of NO_x, we were able

https://doi.org/10.5194/egusphere-2025-2630
Preprint. Discussion started: 8 August 2025

to reasonably reproduce the magnitude and temporal variation of HONO concentrations, especially the higher values observed at noon.

To better understand the mechanisms of HONO formation in the coastal regions of Fujian, we subsequently utilized the SOM process analysis. In general, heterogeneous uptake of NO_2 on the ground surface and NO_x photo-oxidation were two principal contributors to HONO formation, contributing 35–48% and 28–29%, respectively. From 11:00 to 14:00, these two light-dependent reactive pathways led to rapid HONO production rates and offset the effect of lower precursor concentrations, accounting for 64% of the total. Notably, the formed HONO could release OH radicals by self-photolysis, thereby facilitating NO_x photo-oxidation. In spatial, model results suggested that the heterogeneous uptake of NO_2 on the ground surface was more important in forest areas due to the higher density of reactive surface area. In urban areas, high NO_x levels resulted in more HONO production through gas-phase oxidation reactions. We also assessed the impact of shipping emissions on HONO formation in coastal regions by carrying out sensitivity experiments. The model results indicated that shipping emissions contributed to regional increases in NO_x and NO_3^- by 17% and 33%, consequently elevating the average HONO concentration by 18%. The contribution of shipping emissions to HONO decreased from coastal to inland areas. The increased HONO concentrations could be explained by the enhanced production rates. Shipping emissions contributed more evidently to HONO production rates during the daytime, with heterogeneous uptake of NO_2 on the ground surface, NO_x photo-oxidation, NO+OH, and nitrate photolysis accounting for 39%, 34%, 13%, and 12% of the total enhancement, respectively.

Including good HONO source representation significantly led to the rise in concentrations of OH radicals and O_3. The SOM process analysis revealed that photolysis of HONO accounted for 34% of primary OH formation. Meanwhile, this chemical reactive pathway played a more important role in OH formation during the morning rush hours. A sensitivity experiment showed that the diurnal peak of OH levels increased by 61% due to improved representation of HONO sources in the WRF-Chem model. Adjoint SOM analysis of two modeling cases involving BASE and REV further elucidated that only 32% of the increased OH production rate was explained by the direct influence of HONO photolysis; the remainder was contributed by other reactions, including HO_2+NO, O^1D+H_2O, and H_2O_2+hv, due to ambient increased AOC conditions. Consequently, the average O_3 concentration increased by 44% in the coastal regions of Fujian, a much more significant elevation than in previous studies.

Overall, the present study highlights the critical importance of characterizing HONO's formation mechanisms and environmental impacts in coastal regions. Moreover, our study discussed the potential uncertainties regarding HONO simulations in coastal regions, including those arising from the parameterizations of heterogeneous uptake and nitrate photolysis, the estimates of direct emissions from shipping activities, and the unknown impact of the ocean surface.

https://doi.org/10.5194/egusphere-2025-2630
Preprint. Discussion started: 8 August 2025

Therefore, the representative model parameterizations concerning the complicated formation processes of HONO should be continuously developed and coupled into numerical models in the future.

Data availability. The source codes of WRF-Chem model are publicly available on the official website of GitHub (https://github.com/wrf-model/WRF). Meteorological input data for modeling are archived at https://rda.ucar.edu/, with the product codes of d083002, d461000 and d351000 for FNL reanalysis dataset, surface and upper weather observations. Anthropogenic emission inventories of MEIC and SEIM developed by Tsinghua University can be downloaded from the website of http://meicmodel.org.cn/. Other observational and modeling data used in this study are archived on the Figshare platform at https://doi.org/10.6084/m9.figshare.29827070.v1.

Author contributions. XH conceptualized and supervised the study. HRZ performed the model simulations. CYY, SHW and ELN provided the measurement data in Fujian. HRZ and XH analyzed the data and interpreted the results with the help from TYL. HRZ wrote the original manuscript. XH and HRZ revised and edited this paper with contributions from all other co-authors.

Acknowledgements. This study was supported by the Ministry of Science and Technology of the People's Republic of China (2022YFC3701100), the National Natural Science Foundation of China (42293322 and 424B2040), the Natural Science Foundation of Fujian Province (2022J01518 and 2024J01168) and the Comprehensive Observation and Research Project on Atmospheric Pollution in the Meizhou Bay Region.

Competing interests. The contact author has declared that none of the authors has any competing interests.

References

Carter, W. P. L.: "Documentation of the SAPRC-99 Chemical Mechanism for VOC Reactivity Assessment," Report to the California Air resources Board, Contracts 92-329 and 95-308, 2000.

Chen, F. and Dudhia, J.: Coupling and advanced land surface-hydrology model with the Penn State-NCAR MM5 modeling system. Part I: Model implementation and sensitivity, Mon. Weather Rev., 129, 569–585, https://doi.org/10.1175/1520-0493(2001)129<0569:CAALSH>2.0.CO;2, 2001.

Crilley, L. R., Kramer, L. J., Pope, F. D., Reed, C., Lee, J. D., Carpenter, L. J., Hollis, L. D. J., Ball, S. M., and Bloss, W. J.: Is the ocean surface a source of nitrous acid (HONO) in the marine boundary layer?, Atmospheric Chem. Phys., 21, 18213–18225, https://doi.org/10.5194/acp-21-18213-2021, 2021.

Dai, J. and Wang, T.: Impact of international shipping emissions on ozone and $PM_{2.5}$ in East Asia during summer: the important role of HONO and $ClNO_2$, Atmospheric Chem. Phys., 21, 8747–8759, https://doi.org/10.5194/acp-21-8747-2021, 2021.

https://doi.org/10.5194/egusphere-2025-2630
Preprint. Discussion started: 8 August 2025

Finlayson-Pitts, B. J., Wingen, L. M., Sumner, A. L., Syomin, D., and Ramazan, K. A.: The heterogeneous hydrolysis of NO2 in laboratory systems and in outdoor and indoor atmospheres: An integrated mechanism, Phys. Chem. Chem. Phys., 5, 223–242, https://doi.org/10.1039/B208564J, 2003.

Fu, X., Wang, T., Zhang, L., Li, Q., Wang, Z., Xia, M., Yun, H., Wang, W., Yu, C., Yue, D., Zhou, Y., Zheng, J., and Han, R.: The significant contribution of HONO to secondary pollutants during a severe winter pollution event in southern China, Atmospheric Chem. Phys., 19, 1–14, https://doi.org/10.5194/acp-19-1-2019, 2019.

George, C., Ammann, M., D'Anna, B., Donaldson, D. J., and Nizkorodov, S. A.: Heterogeneous Photochemistry in the Atmosphere, Chem. Rev., 115, 4218–4258, https://doi.org/10.1021/cr500648z, 2015.

Grell, G. A. and Dévényi, D.: A generalized approach to parameterizing convection combining ensemble and data assimilation techniques, Geophys. Res. Lett., 29, https://doi.org/10.1029/2002GL015311, 2002.

Grell, G. A., Peckham, S. E., Schmitz, R., McKeen, S. A., Frost, G., Skamarock, W. C., and Eder, B.: Fully coupled "online" chemistry within the WRF model, Atmos. Environ., 39, 6957–6975, https://doi.org/10.1016/j.atmosenv.2005.04.027, 2005.

Guenther, A., Karl, T., Harley, P., Wiedinmyer, C., Palmer, P. I., and Geron, C.: Estimates of global terrestrial isoprene emissions using MEGAN (Model of Emissions of Gases and Aerosols from Nature), Atmospheric Chem. Phys., 6, 3181–3210, https://doi.org/10.5194/acp-6-3181-2006, 2006.

Guo, Y., Zhang, J., An, J., Qu, Y., Liu, X., Sun, Y., and Chen, Y.: Effect of vertical parameterization of a missing daytime source of HONO on concentrations of HONO, O3 and secondary organic aerosols in eastern China, Atmos. Environ., 226, 117208, https://doi.org/10.1016/j.atmosenv.2019.117208, 2020.

Hong, S.-Y., Noh, Y., and Dudhia, J.: A New Vertical Diffusion Package with an Explicit Treatment of Entrainment Processes, https://doi.org/10.1175/MWR3199.1, 2006.

Hu, B., Duan, J., Hong, Y., Xu, L., Li, M., Bian, Y., Qin, M., Fang, W., Xie, P., and Chen, J.: Exploration of the atmospheric chemistry of nitrous acid in a coastal city of southeastern China: results from measurements across four seasons, Atmospheric Chem. Phys., 22, 371–393, https://doi.org/10.5194/acp-22-371-2022, 2022.

Iacono, M. J., Delamere, J. S., Mlawer, E. J., Shephard, M. W., Clough, S. A., and Collins, W. D.: Radiative forcing by long-lived greenhouse gases: Calculations with the AER radiative transfer models, J. Geophys. Res. Atmospheres, 113, https://doi.org/10.1029/2008JD009944, 2008.

Jiang, Y., Xue, L., Gu, R., Jia, M., Zhang, Y., Wen, L., Zheng, P., Chen, T., Li, H., Shan, Y., Zhao, Y., Guo, Z., Bi, Y., Liu, H., Ding, A., Zhang, Q., and Wang, W.: Sources of nitrous acid (HONO) in the upper boundary layer and lower free troposphere of the North China Plain: insights from the Mount Tai Observatory, Atmospheric Chem. Phys., 20, 12115–12131, https://doi.org/10.5194/acp-20-12115-2020, 2020.

Jiang, Y., Xia, M., Xue, L., Wang, X., Zhong, X., Liu, Y., Kulmala, M., Ma, T., Wang, J., Wang, Y., Gao, J., and Wang, T.: Quantifying HONO Production from Nitrate Photolysis in a Polluted Atmosphere, Environ. Sci. Technol., https://doi.org/10.1021/acs.est.4c06061, 2024.

Jiménez, P. A., Dudhia, J., González-Rouco, J. F., Navarro, J., Montávez, J. P., and García-Bustamante, E.: A revised scheme for the WRF surface layer formulation, Mon. Weather Rev., 140, 898–918, https://doi.org/10.1175/MWR-D-11-00056.1, 2012.

https://doi.org/10.5194/egusphere-2025-2630
Preprint. Discussion started: 8 August 2025

Ke, J., Yang, X., Lu, K., Fu, M., Wang, Y., Yin, H., and Ding, Y.: Overlooked Underestimation of Mobile Sources Posing a Pronounced Imbalance in the HONO Budget, Environ. Sci. Technol., 59, 5875–5877, https://doi.org/10.1021/acs.est.5c02684, 2025.

Kim, K., Han, K. M., Song, C. H., Lee, H., Beardsley, R., Yu, J., Yarwood, G., Koo, B., Madalipay, J., Woo, J.-H., and Cho, S.: An investigation into atmospheric nitrous acid (HONO) processes in South Korea, Atmospheric Chem. Phys., 24, 12575–12593, https://doi.org/10.5194/acp-24-12575-2024, 2024.

Kleffmann, J., Gavriloaiei, T., Hofzumahaus, A., Holland, F., Koppmann, R., Rupp, L., Schlosser, E., Siese, M., and Wahner, A.: Daytime formation of nitrous acid: A major source of OH radicals in a forest, Geophys. Res. Lett., 32, https://doi.org/10.1029/2005GL022524, 2005.

Kurtenbach, R., Becker, K. H., Gomes, J. A. G., Kleffmann, J., Lörzer, J. C., Spittler, M., Wiesen, P., Ackermann, R., Geyer, A., and Platt, U.: Investigations of emissions and heterogeneous formation of HONO in a road traffic tunnel, Atmos. Environ., 35, 3385–3394, https://doi.org/10.1016/S1352-2310(01)00138-8, 2001.

Li, M., Zhang, Q., Kurokawa, J., Woo, J.-H., He, K., Lu, Z., Ohara, T., Song, Y., Streets, D. G., Carmichael, G. R., Cheng, Y., Hong, C., Huo, H., Jiang, X., Kang, S., Liu, F., Su, H., and Zheng, B.: MIX: a mosaic Asian anthropogenic emission inventory under the international collaboration framework of the MICS-Asia and HTAP, Atmospheric Chem. Phys., 17, 935–963, https://doi.org/10.5194/acp-17-935-2017, 2017.

Li, X., Bei, N., Wu, J., Wang, R., Liu, S., Liu, L., Jiang, Q., Tie, X., Molina, L. T., and Li, G.: Heterogeneous HONO formation deteriorates the wintertime particulate pollution in the Guanzhong Basin, China, Environ. Pollut., 303, 119157, https://doi.org/10.1016/j.envpol.2022.119157, 2022.

Lin, Y.-L., Farley, R. D., and Orville, H. D.: Bulk Parameterization of the Snow Field in a Cloud Model, 1983.

Liu, H., Fu, M., Jin, X., Shang, Y., Shindell, D., Faluvegi, G., Shindell, C., and He, K.: Health and climate impacts of ocean-going vessels in East Asia, Nat. Clim. Change, 6, 1037–1041, https://doi.org/10.1038/nclimate3083, 2016.

Liu, Y., Lu, K., Li, X., Dong, H., Tan, Z., Wang, H., Zou, Q., Wu, Y., Zeng, L., Hu, M., Min, K.-E., Kecorius, S., Wiedensohler, A., and Zhang, Y.: A Comprehensive Model Test of the HONO Sources Constrained to Field Measurements at Rural North China Plain, Environ. Sci. Technol., 53, 3517–3525, https://doi.org/10.1021/acs.est.8b06367, 2019.

Oswald, R., Behrendt, T., Ermel, M., Wu, D., Su, H., Cheng, Y., Breuninger, C., Moravek, A., Mougin, E., Delon, C., Loubet, B., Pommerening-Röser, A., Sörgel, M., Pöschl, U., Hoffmann, T., Andreae, M. O., Meixner, F. X., and Trebs, I.: HONO Emissions from Soil Bacteria as a Major Source of Atmospheric Reactive Nitrogen, Science, 341, 1233–1235, https://doi.org/10.1126/science.1242266, 2013.

Ran, H., An, J., Zhang, J., Huang, J., Qu, Y., Chen, Y., Xue, C., Mu, Y., and Liu, X.: Impact of soil–atmosphere HONO exchange on concentrations of HONO and O3 in the North China Plain, Sci. Total Environ., 928, 172336, https://doi.org/10.1016/j.scitotenv.2024.172336, 2024.

Sarwar, G., Roselle, S. J., Mathur, R., Appel, W., Dennis, R. L., and Vogel, B.: A comparison of CMAQ HONO predictions with observations from the Northeast Oxidant and Particle Study, Atmos. Environ., 42, 5760–5770, https://doi.org/10.1016/j.atmosenv.2007.12.065, 2008.

Seinfeld, J. H. and Pandis, S. N.: Atmospheric Chemistry and Physics: From Air Pollution to Climate Change, John Wiley & Sons, Hoboken, New Jersey, 2016.

https://doi.org/10.5194/egusphere-2025-2630
Preprint. Discussion started: 8 August 2025

Song, M., Zhao, X., Liu, P., Mu, J., He, G., Zhang, C., Tong, S., Xue, C., Zhao, X., Ge, M., and Mu, Y.: Atmospheric NOx oxidation as major sources for nitrous acid (HONO), Npj Clim. Atmospheric Sci., 6, 30, https://doi.org/10.1038/s41612-023-00357-8, 2023.

Su, H., Cheng, Y., Oswald, R., Behrendt, T., Trebs, I., Meixner, F. X., Andreae, M. O., Cheng, P., Zhang, Y., and Pöschl, U.: Soil Nitrite as a Source of Atmospheric HONO and OH Radicals, Science, 333, 1616–1618, https://doi.org/10.1126/science.1207687, 2011.

Sun, L., Chen, T., Jiang, Y., Zhou, Y., Sheng, L., Lin, J., Li, J., Dong, C., Wang, C., Wang, X., Zhang, Q., Wang, W., and Xue, L.: Ship emission of nitrous acid (HONO) and its impacts on the marine atmospheric oxidation chemistry, Sci. Total Environ., 735, 139355, https://doi.org/10.1016/j.scitotenv.2020.139355, 2020.

Tan, W., Wang, H., Su, J., Sun, R., He, C., Lu, X., Lin, J., Xue, C., Wang, H., Liu, Y., Liu, L., Zhang, L., Wu, D., Mu, Y., and Fan, S.: Soil Emissions of Reactive Nitrogen Accelerate Summertime Surface Ozone Increases in the North China Plain, Environ. Sci. Technol., 57, 12782–12793, https://doi.org/10.1021/acs.est.3c01823, 2023.

Wang, L., Chai, J., Gaubert, B., and Huang, Y.: A review of measurements and model simulations of atmospheric nitrous acid, Atmos. Environ., 347, 121094, https://doi.org/10.1016/j.atmosenv.2025.121094, 2025.

Wang, T., Xue, L., Brimblecombe, P., Lam, Y. F., Li, L., and Zhang, L.: Ozone pollution in China: A review of concentrations, meteorological influences, chemical precursors, and effects, Sci. Total Environ., 575, 1582–1596, https://doi.org/10.1016/j.scitotenv.2016.10.081, 2017.

Wild, O., Zhu, X., and Prather, M. J.: Fast-J: Accurate Simulation of In- and Below-Cloud Photolysis in Tropospheric Chemical Models, J. Atmospheric Chem., 37, 245–282, https://doi.org/10.1023/A:1006415919030, 2000.

Xue, C.: Substantially Growing Interest in the Chemistry of Nitrous Acid (HONO) in China: Current Achievements, Problems, and Future Directions, Environ. Sci. Technol., 56, 7375–7377, https://doi.org/10.1021/acs.est.2c02237, 2022.

Xue, C., Ye, C., Kleffmann, J., Zhang, C., Catoire, V., Bao, F., Mellouki, A., Xue, L., Chen, J., Lu, K., Zhao, Y., Liu, H., Guo, Z., and Mu, Y.: Atmospheric measurements at Mt. Tai – Part I: HONO formation and its role in the oxidizing capacity of the upper boundary layer, Atmospheric Chem. Phys., 22, 3149–3167, https://doi.org/10.5194/acp-22-3149-2022, 2022.

Xue, C., Chen, H., McGillen, M. R., Su, H., Cheng, Y., Kleffmann, J., Li, G., Cazaunau, M., Colomb, A., Sciare, J., DeWitt, L., Marchand, N., Sarda-Esteve, R., Petit, J.-E., and Kukui, A.: Role of Heterogeneous Reactions in the Atmospheric Oxidizing Capacity in Island Environments, Environ. Sci. Technol., 59, 3153–3164, https://doi.org/10.1021/acs.est.4c11647, 2025.

Yang, X., Lu, K., Ma, X., Liu, Y., Wang, H., Hu, R., Li, X., Lou, S., Chen, S., Dong, H., Wang, F., Wang, Y., Zhang, G., Li, S., Yang, S., Yang, Y., Kuang, C., Tan, Z., Chen, X., Qiu, P., Zeng, L., Xie, P., and Zhang, Y.: Observations and modeling of OH and HO2 radicals in Chengdu, China in summer 2019, Sci. Total Environ., 772, 144829, https://doi.org/10.1016/j.scitotenv.2020.144829, 2021.

Ye, C., Zhou, X., Pu, D., Stutz, J., Festa, J., Spolaor, M., Tsai, C., Cantrell, C., Mauldin, R. L., Campos, T., Weinheimer, A., Hornbrook, R. S., Apel, E. C., Guenther, A., Kaser, L., Yuan, B., Karl, T., Haggerty, J., Hall, S., Ullmann, K., Smith, J. N., Ortega, J., and Knote, C.: Rapid cycling of reactive nitrogen in the marine boundary layer, Nature, 532, 489–491, https://doi.org/10.1038/nature17195, 2016.

Ye, C., Zhang, N., Gao, H., and Zhou, X.: Photolysis of Particulate Nitrate as a Source of HONO and NOx, Environ. Sci. Technol., 51, 6849–6856, https://doi.org/10.1021/acs.est.7b00387, 2017.

https://doi.org/10.5194/egusphere-2025-2630
Preprint. Discussion started: 8 August 2025

Ye, C., Lu, K., Ma, X., Qiu, W., Li, S., Yang, X., Xue, C., Zhai, T., Liu, Y., Li, X., Li, Y., Wang, H., Tan, Z., Chen, X., Dong, H., Zeng, L., Hu, M., and Zhang, Y.: HONO chemistry at a suburban site during the EXPLORE-YRD campaign in 2018: formation mechanisms and impacts on O_3 production, Atmospheric Chem. Phys., 23, 15455–15472, https://doi.org/10.5194/acp-23-15455-2023, 2023.

Zaveri, R. A., Easter, R. C., Fast, J. D., and Peters, L. K.: Model for Simulating Aerosol Interactions and Chemistry (MOSAIC), J. Geophys. Res., 113, D13204, https://doi.org/10.1029/2007JD008782, 2008.

Zha, Q., Xue, L., Wang, T., Xu, Z., Yeung, C., Louie, P. K. K., and Luk, C. W. Y.: Large conversion rates of NO2 to HNO2 observed in air masses from the South China Sea: Evidence of strong production at sea surface?, Geophys. Res. Lett., 41, 7710–7715, https://doi.org/10.1002/2014GL061429, 2014.

Zhang, H., Zhou, X., Ren, C., Li, M., Liu, T., and Huang, X.: A systematic review of reactive nitrogen simulations with chemical transport models in China, Atmospheric Res., 107586, https://doi.org/10.1016/j.atmosres.2024.107586, 2024a.

Zhang, H., Ren, C., Zhou, X., Tang, K., Liu, Y., Liu, T., Wang, J., Chi, X., Li, M., Li, N., Huang, X., and Ding, A.: Improving HONO Simulations and Evaluating Its Impacts on Secondary Pollution in the Yangtze River Delta Region, China, J. Geophys. Res. Atmospheres, 129, e2024JD041052, https://doi.org/10.1029/2024JD041052, 2024b.

Zhang, J., Lian, C., Wang, W., Ge, M., Guo, Y., Ran, H., Zhang, Y., Zheng, F., Fan, X., Yan, C., Daellenbach, K. R., Liu, Y., Kulmala, M., and An, J.: Amplified role of potential HONO sources in O3 formation in North China Plain during autumn haze aggravating processes, Atmospheric Chem. Phys., 22, 3275–3302, https://doi.org/10.5194/acp-22-3275-2022, 2022a.

Zhang, J., Ran, H., Guo, Y., Xue, C., Liu, X., Qu, Y., Sun, Y., Zhang, Q., Mu, Y., Chen, Y., Wang, J., and An, J.: High crop yield losses induced by potential HONO sources — A modelling study in the North China Plain, Sci. Total Environ., 803, 149929, https://doi.org/10.1016/j.scitotenv.2021.149929, 2022b.

Zhang, L., Wang, T., Zhang, Q., Zheng, J., Xu, Z., and Lv, M.: Potential sources of nitrous acid (HONO) and their impacts on ozone: A WRF-Chem study in a polluted subtropical region, J. Geophys. Res. Atmospheres, 121, 3645–3662, https://doi.org/10.1002/2015JD024468, 2016.

Zhang, L., Li, Q., Wang, T., Ahmadov, R., Zhang, Q., Li, M., and Lv, M.: Combined impacts of nitrous acid and nitryl chloride on lower-tropospheric ozone: new module development in WRF-Chem and application to China, Atmospheric Chem. Phys., 17, 9733–9750, https://doi.org/10.5194/acp-17-9733-2017, 2017.

Zhang, S., Sarwar, G., Xing, J., Chu, B., Xue, C., Sarav, A., Ding, D., Zheng, H., Mu, Y., Duan, F., Ma, T., and He, H.: Improving the representation of HONO chemistry in CMAQ and examining its impact on haze over China, Atmospheric Chem. Phys., 21, 15809–15826, https://doi.org/10.5194/acp-21-15809-2021, 2021.

Zhang, X., Tong, S., Jia, C., Zhang, W., Li, J., Wang, W., Sun, Y., Wang, X., Wang, L., Ji, D., Wang, L., Zhao, P., Tang, G., Xin, J., Li, A., and Ge, M.: The Levels and Sources of Nitrous Acid (HONO) in Winter of Beijing and Sanmenxia, J. Geophys. Res. Atmospheres, 127, e2021JD036278, https://doi.org/10.1029/2021JD036278, 2022c.

Zhang, X., Tong, S., Jia, C., Zhang, W., Wang, Z., Tang, G., Hu, B., Liu, Z., Wang, L., Zhao, P., Pan, Y., and Ge, M.: Elucidating HONO formation mechanism and its essential contribution to OH during haze events, Npj Clim. Atmospheric Sci., 6, 55, https://doi.org/10.1038/s41612-023-00371-w, 2023.

Zheng, B., Tong, D., Li, M., Liu, F., Hong, C., Geng, G., Li, H., Li, X., Peng, L., Qi, J., Yan, L., Zhang, Y., Zhao, H., Zheng, Y., He, K., and Zhang, Q.: Trends in China's anthropogenic emissions since 2010 as the consequence of clean air actions, Atmospheric Chem. Phys., 18, 14095–14111, https://doi.org/10.5194/acp-18-14095-2018, 2018.

https://doi.org/10.5194/egusphere-2025-2630
Preprint. Discussion started: 8 August 2025

655 Zhong, X., Shen, H., Zhao, M., Zhang, J., Sun, Y., Liu, Y., Zhang, Y., Shan, Y., Li, H., Mu, J., Yang, Y., Nie, Y., Tang, J., Dong, C., Wang, X., Zhu, Y., Guo, M., Wang, W., and Xue, L.: Nitrous acid budgets in the coastal atmosphere: potential daytime marine sources, Atmospheric Chem. Phys., 23, 14761–14778, https://doi.org/10.5194/acp-23-14761-2023, 2023.